JMEPEG (2005) 14:99-103
DOI: 10.1361/10599490522185

1059-9495/$19.00

Effect of Manganese Substitution on the Magnetic Properties of Nickel-Zinc Ferrite

A.A. Sattar, H.M. El-Sayed, K.M. El-Shokrofy, and M.M. El-Tabey

(Submitted December 9, 2003)

The effect of manganese (Mn)-ion substitution on the structural, magnetic, and electrical properties of nickel-zinc (Ni-Zn) ferrite of chemical formula $Ni_{0.6-t}$ Mn_t $Zn_{0.4}Fe_2O_4$ (t = 0.0, 0.1, 0.2, 0.3, 0.4, 0.45, 0.5, 0.55, 0.6) has been studied. It was found that Mn ion substitution increases the average grain diameter and improves the magnetization as well as the initial permeability. At the same time, the direct current (dc) resistivity at room temperature was found to increase with Mn ion substitution. The increase of both magnetization and dc resistivity due to the Mn substitution in a Ni-Zn ferrite is a promising result for applications in high-frequency fields.

Keywords electrical properties, ferrites, magnetic properties, manganese-nickel-zinc ferrites, microstructure

1. Introduction

Nickel-zinc (Ni-Zn) ferrite is one of the most popular soft ferrites that is used commercially due to its important magnetic and electrical properties. This ferrite has been extensively used as a magnetic core material for a large number of devices and electrical components, such as phase shifters, circulators, isolators, inductors, transformers, and computer memories. The dependence of the magnetic and electrical properties of Ni-Zn ferrites on the composition and temperature has been extensively studied (Ref 1-3). The effect of copper (Cu), titanium, and lithium-ion substitutions on the electrical and magnetic properties of Ni-Zn ferrites also has been studied (Ref 4-9). Dionne and West (Ref 9) investigated the effect of manganese-iron (Mn-Fe) substitution on the magnetic properties in Ni-Zn ferrite. They found that the saturation magnetization and Curie temperature (T_C) decreased with increasing Mn ion concentration. In the present work, the effect of Mn-Ni substitution on the structural and magnetic properties of Ni-Zn ferrite was investigated.

2. Experimental Procedure

Ferrite samples with the chemical formula $Ni_{0.6-t}$ Mn_t $Zn_{0.4}Fe_2O_4$ (t = 0, 0.1, 0.2, 0.3, 0.4, 0.45, 0.5, 0.55, 0.6) were prepared by conventional ceramic processing methods. High-purity oxides (99.99%) of NiO, ZnO, and Fe_2O_3 with $MnCO_3$ were mixed together according to their molecular weights. The mixture of each composition was ground to a very fine powder and presintered at 900 °C for 15 h. The presintered mixture was ground again and pressed at room temperature under a pressure of 3.8×10^8 Pa into tablet and toroidal forms. They were finally sintered at 1300 °C for 4 h in two cycles and then slowly cooled at a rate 1 °C/min in N_2 atmosphere to room temperature.

X-ray diffraction patterns were generated using a diffractometer with Cu K_α radiation. The theoretical x-ray density (d_x) of the samples was calculated using the formula ($d_x = 8M/Na^3$) where M is the molecular weight, N is Avogadro's number, and a is the lattice parameter. The density d of each composition was measured in toluene using the Archimedes principle. The porosity percentage (P %) was calculated according to the relation $p = 100\,[1 - (d/d_x)]\%$. The grain size was obtained by using scanning electron microscopy. From these micrographs, the average grain size was calculated. The magnetization (emu/gm) was measured by using the vibrating sample technique. The magnetizing field ranges from 0 up to 0.9 T. Toroidal-shaped samples were used as transformer cores for measuring the initial permeability; the inner diameter was equal to 0.75 cm, the outer diameter was equal to 1.55 cm, and the average thickness was equal to ~0.3 cm. The initial permeability, μ_i, was measured as a function of temperature at a constant frequency (f = 10 KHz) of the sinusoidal wave. The magnetizing current in the primary coil, I_p, was kept constant at 4 mA. The value of μ_i was calculated using Poltinnikov's formula (Ref 10). According to this formula $V_S = K\mu_i$, where V_S is the induced voltage in the secondary coil, and $K = 0.4\,\Pi\, I_P N_P N_S A\omega/L$, where N_P and N_S are the number of turns of primary and secondary coils, respectively ($N_P = N_S = 15$ turns), A is the cross-section area of the sample, ω is the angular frequency, and L is the average path of the magnetic flux.

3. Results and Discussion

3.1 Physical Properties

The x-ray diffraction patterns showed that all samples consisted of the cubic single spinel phase. The interplanar spacing was calculated according to Bragg's law as well as the average lattice constant (a). The theoretical lattice constant is calculated using (Ref 11):

$$a_{th} = \frac{8}{3\sqrt{3}}\left[(r_A + R_o) + \sqrt{3}\,(r_B + R_o)\right] \quad \text{(Eq 1)}$$

A.A. Sattar and **H.M. El-Sayed,** Physics Department, Faculty of Science, Ain Shams University, Cairo, Egypt; and **K.M. El-Shokrofy** and **M.M. El-Tabey,** Physics and Mathematical Engineering Department, Faculty of Engineering, Menoufia University, Shebin El-Kom, Egypt. Contact e-mail: adel_sattar@hotmail.com.

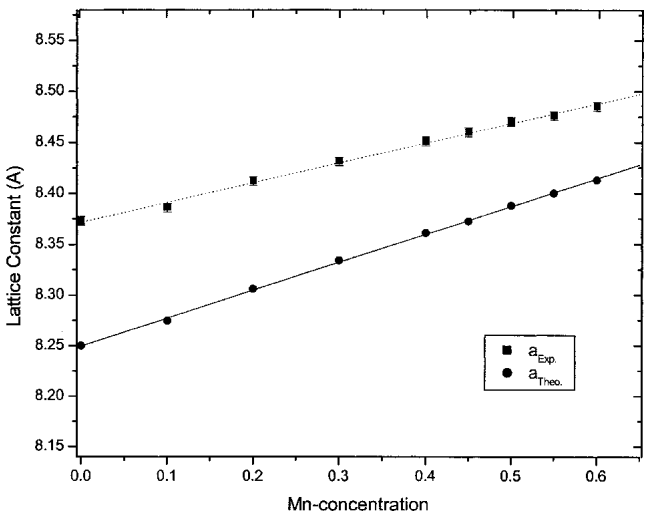

Fig. 1 The variation of the lattice constant a (Å) with Mn concentration (t)

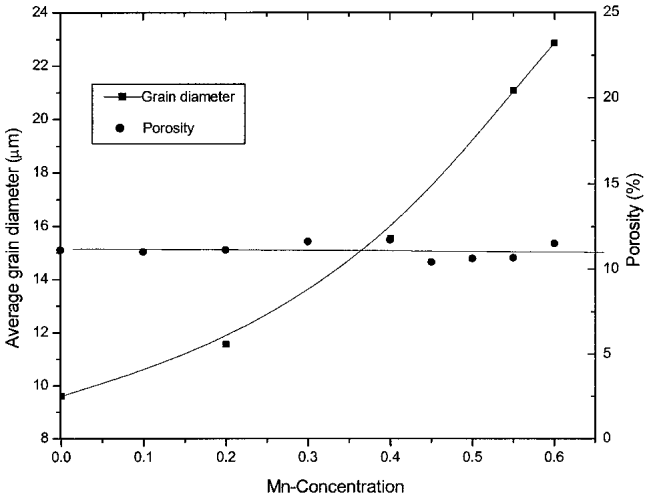

Fig. 2 Change of porosity (P%) and the average grain diameter D (μm) with Mn concentration

where R_o is the radius of the oxygen ion (1.32 Å), and r_A and r_B are the ionic radii of tetrahedral and octahedral sites, respectively. To calculate r_A and r_B, the following cation distribution was assumed:

$$(Zn_{0.4}\ Mn_{0.8t}\ Fe_{0.6-0.8t})\ [Mn_{0.2t}\ Ni_{0.6-t}\ Fe_{1.4+0.8t}]\ O_4$$

This cation distribution is based on the premise that 80% of Mn ions occupy the tetrahedral position (i.e., the A site), while the remaining 20% occupy the octahedral position (i.e., the B site) (Ref 12). Moreover, Zn ions preferentially occupy the tetrahedral sites, whereas the Ni ions occupy the octahedral sites. The ionic radius for each site was calculated according to (Ref 11):

$$r_A = [(0.4)\ r_{Zn^{2+}} + (0.8\ t)\ r_{Mn^{2+}} + (0.6 - (0.8\ t))\ r_{Fe^{3+}}]$$

$$r_B = [(0.2\ t)\ r_{Mn^{2+}} + (0.6 - t)\ r_{Ni^{2+}} + (1.4 + (0.8\ t))\ r_{Fe^{3+}}]/2$$

The values of $r_{Zn^{2+}}$, $r_{Mn^{2+}}$, $r_{Fe^{3+}}$, and $r_{Ni^{2+}}$ are the ionic radii of Zn, Mn, Fe, and Ni, respectively. These values are taken from Ref 13, in which the ionic radius depends on its coordination number. Figure 1 shows the variation of the experimental and theoretical lattice constants with Mn concentration for all samples. It is informative to note that the lattice constant for the nonsubstituted sample (i.e., the $t = 0$ sample) is 8.373 Å, which is in agreement with values previously reported (8.384 (Ref 1) and 8.381 Å (Ref 14). It is clear that the lattice constant increases linearly with Mn concentration and obeys Vegard's law. Such behavior can be attributed to the replacement of the Ni^{2+} ion, which has a radius of 0.72 Å, by the Mn^{2+} ion, which has a radius a little larger than 0.8 Å. Additionally, the experimental values of the lattice constant are greater than those of the theoretical values, and the difference between them decreases with increasing Mn concentration. This can be attributed to the formation of Fe^{2+} ions, which have an ionic radius greater than Fe^{3+}.

The variation in porosity and the grain size with Mn concentration of all samples is shown in Fig. 2. In this case, the porosity is almost constant with increasing Mn concentration, whereas the average grain diameter increased. This could be explained as follows: It is well-known that the porosity of ceramic samples results from two sources, intragranular porosity (P_{intra}) and intergranular porosity (P_{inter}) (Ref 15). Thus, the total porosity P is the sum of the two types, that is, $P = (P_{intra} + P_{inter})$. Furthermore, it was reported that as the grain size increases the intergranular porosity increases (Ref 16). Therefore, the constancy of the total porosity leads to the conclusion that the intragranular porosity decreases with increasing the Mn concentration.

3.2 Magnetic Properties

3.2.1 Magnetization and Coercive Field. Figure 3 shows the change in magnetization with the applied magnetic field (H up to 0.9 T) for all samples at 77 K. As in normal behavior, the magnetization increases with increasing applied magnetic field and attains its saturation value for fields higher than 0.6 T. The saturation magnetization M_s is determined by extrapolating the magnetization curve to $H = 0$. The dependence of the saturation magnetization M_s on Mn concentration is shown in Fig. 4. It is clear that as the Mn ion concentration increases, the saturation magnetization increases rapidly up to a concentration of 0.45, but for concentrations >0.45, the magnetization increases only slightly. The increase of M_s with increasing concentration can be explained according to the cation distribution. It is clear that as the Mn concentration increases, the magnetization of the B-site (M_B) increases while that of the A-site (M_A) remains constant. As the net magnetization (M_s) equals ($M_B - M_A$) and should increase with increasing Mn concentration. This is found to be the case for concentrations up to 0.45. The slight increase in magnetization for concentrations >0.45 can be attributed to two factors:

- The increase of canting angle between the moments in the B-site leads to a decrease in the magnetization (Ref 17).

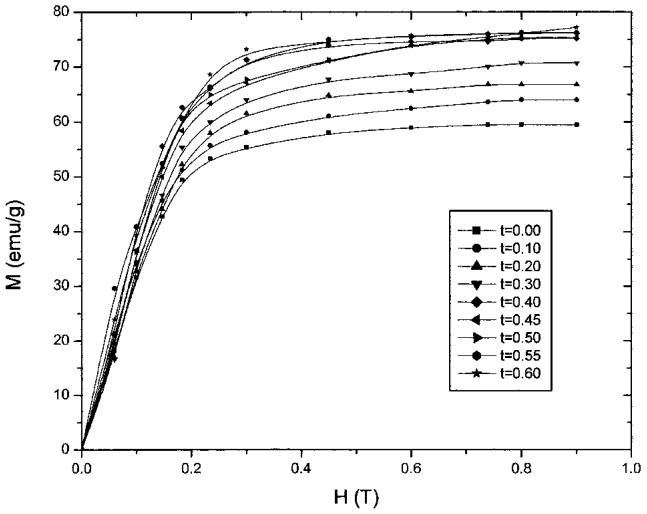

Fig. 3 The magnetization M (emu/g) versus the applied magnetic field H (T)

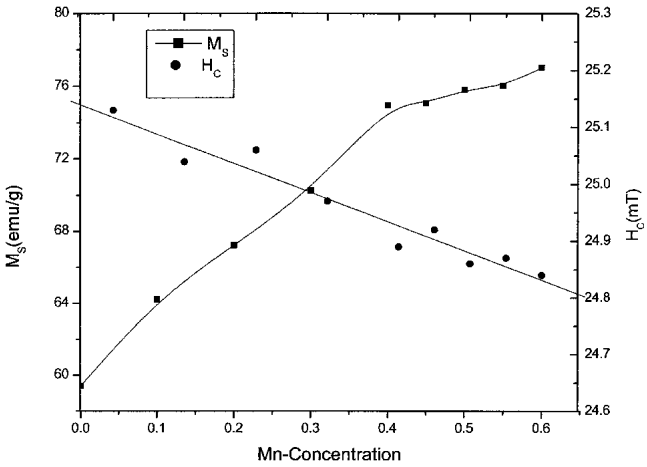

Fig. 4 The variation of saturation magnetization M_s (emu/g) and coercive force H_c (mT) with Mn concentration (t)

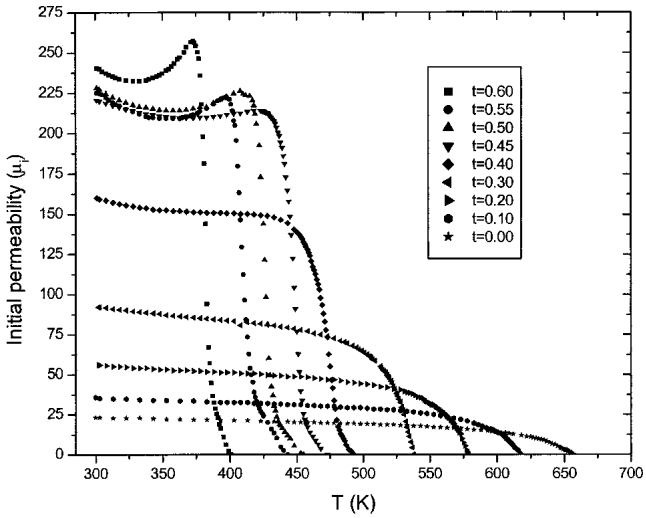

Fig. 5 The temperature dependence of the initial permeability μ_i

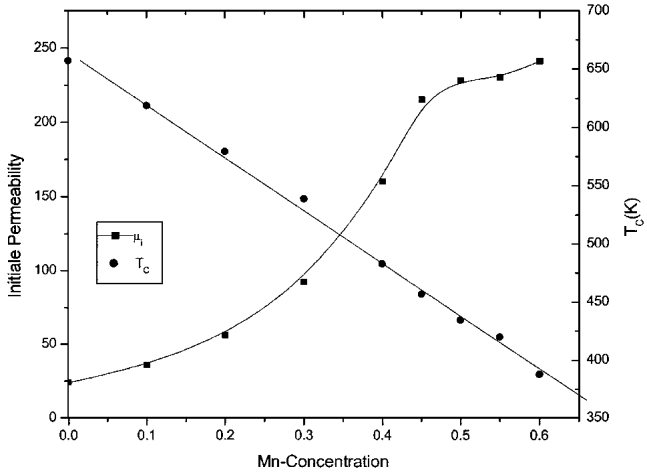

Fig. 6 The variation of the initial permeability μ_i (at room temperature) and T_C (K) with the Mn concentration (t)

- The increase in the magnitude of the total magnetic moments in the B-site leads to a magnetization increase.

These two factors seem to compete with each other such that M_s increases only slightly for concentrations >0.45.

Figure 4 shows the change in the coercive force (H_c) with Mn ion concentration. It is obvious that the magnitude of H_c decreases with increasing Mn content. This may be explained as follows: It is known that the coercive force has a direct relation with the anisotropy constant of the sample, and, according to the one-ion model, the anisotropy field of ferrites depends on the amount of Fe^{2+} ions in the sample (Ref 18). From the previous discussion on x-ray measurements, it seems that the amount of Fe^{2+} ions decreases as a result of increasing Mn content. This means that the anisotropy constant decreases with increasing Mn content and that, consequently, the magnitude of H_c also decreases.

3.2.2 Initial Permeability and Curie Temperature. The variation of the initial permeability μ_i with temperature is shown in Fig. 5. It was found that the curves are typical of multidomain grains showing a sudden drop in μ_i at T_C. The T_C is determined by drawing a tangent to the curve at the point of rapid decrease in μ_i. The intersection of the tangent with the temperature axis determines T_C. The sharp decrease in μ_i with temperature at T_C reflects the homogeneity of the sample (Ref 19). It is obvious that as the Mn concentration increases, the sharpness of the curve increases (i.e., the homogeneity increases). This can be attributed to the increase in the average grain size of the ferrite as Mn concentration increases. Figure 6 shows the dependence of initial permeability μ_i on the Mn concentration at room temperature. It is obvious that the variation in μ_i with Mn concentration increases more rapidly for concentrations $\leq$0.45 than for those >0.45. This behavior can be explained using the following approximate equation for the initial permeability (Ref 20):

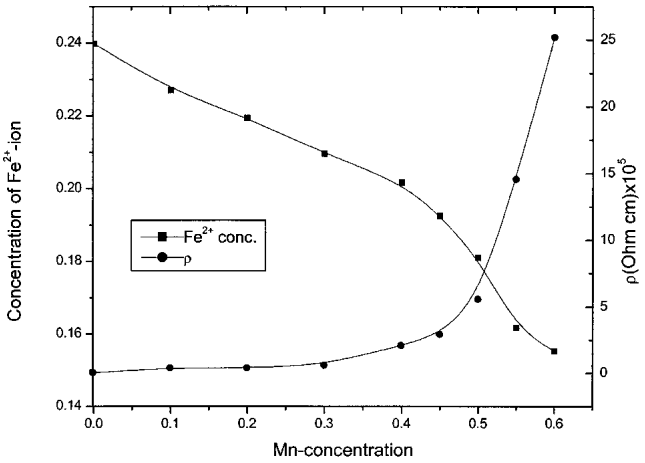

Fig. 7 The dependence of the resistivity ρ (at room temperature) and Fe^{2+} ion concentration on the Mn concentration (*t*)

$$\mu_i \approx \frac{M_S^2 D}{\sqrt{K_1}} \qquad \text{(Eq 2)}$$

where M_S is the saturation magnetization, D is the average grain diameter, and K_1 is the magnetocrystalline anisotropy constant. According to the above results, both M and average grain diameter increase as Mn content increases. This leads to an increase in the value of μ_i. Furthermore, it was also reported that the anisotropy constant for Ni-Zn ferrite ($K_1 = -1.7 \times 10^3$ J/m^3) is greater than that of Mn-Zn ferrite ($K_1 = -0.2 \times 10^3$ J/m^3) (Ref 21). This means that as the Mn concentration increases, the anisotropy constant (K_1) decreases, and thus the initial permeability also increases. Therefore, all the parameters in Eq 2 are responsible for the rapid increase in μ_i for concentrations ≤ 0.45. On the other hand, for samples with concentrations >0.45, according to Eq 2, μ_i depends on the square of M_s, but M_s only slightly increases with concentration. So M_s seems to dominate over D and K_1, leading to the slight increase in μ_i with increasing concentration.

Figure 6 shows the change in T_C with Mn concentration. It is seen that as Mn concentration increases, T_C decreases. This can be explained as follows. It is known that the T_C depends mainly on A-B interactions. In these samples, as mentioned above, an increase in the Mn concentration causes an increase in the lattice parameter. This means that the distances between the ions increase, which leads the different A-B interactions to decrease. Also, according to Ref 22, the exchange integral [$J_{Fe^{3+}(A)\text{-}Ni^{2+}(B)} = (-27.4\ K)$] is greater than [$J_{Fe^{3+}(A)\text{-}Mn^{2+}(B)} = (-19.1\ K)$], which causes the A-B interactions to decrease, and hence, the T_C also decreases.

3.2.3 Resistivity at Room Temperature. Figure 7 shows the variation in electrical resistivity (ρ) at room temperature as a function of the Mn ion concentration. It is clear that the substitution of Mn ions leads to an increase in the resistivity of all samples. This behavior can be interpreted in terms of the formation of Fe^{2+} ions due to the oxygen loss during the sintering process. The concentration of Fe^{2+} ions in each sample is estimated from the difference between the experimental and theoretical values of the lattice constants. The change in Fe^{2+} concentration with Mn content is also shown in Fig. 7. It should be noted that as the Mn concentration increases, the concentration of Fe^{2+} decreases, which is in agreement with the fact that Mn ions cause the suppression of Fe^{2+} ion formation (Ref 23). Therefore, as the ferrous ion concentration decreases, the hopping between Fe^{3+} and Fe^{2+} decreases, which leads to an increase in the resistivity.

4. Conclusions

- The substitution of Mn ions into Ni-Zn ferrite greatly affected the physical properties, with the lattice parameter and the average grain size increasing. The intragranular porosity also increased at the expense of the intergranular porosity.
- The magnetic properties of Mn-substituted Ni-Zn ferrites improved with increases in both magnetization and initial permeability. The electrical resistivity of the samples also increased. These results are promising for high-frequency applications.

References

1. A. Globus, H. Pascaer, and V. Cagan, Distance Between Magnetic Ions and Fundamental Properties in Ferrites, *J. Phys. Coll. C1,* Vol 38 (suppl.), 1977, p C1-C163
2. H. Igarashi and K. Okazaki, Effect of Porosity and Grain Size on the Magnetic Properties of Ni-Zn Ferrite, *J. Am. Ceram. Soc.,* Vol 60 (No. 1-2), 1976, p 51-54
3. S.R. Murthy, "A Study of Microwave Absorbing Properties of Nano-Particles Ni-Zn Ferrites," presented at Eighth International Conference on Ferrites (ICF8) September 18, The Japan Society of Powder and Powder Metallurgy (Kyoto and Tokyo, Japan), 2000
4. G. K. Joshi, A.Y. Khot, and S.R. Swant, Electrical Conductivity Studies of Copper-Substituted and Non-Substituted Ni-Zn Mixed Ferrites, *J. Mater. Sci.,* Vol 22, 1984, p 1694-1700
5. D.C. Khan, M. Misra, and A.R. Das, Structure and Magnetization Studies of Ti-Substituted $Ni_{0.3}Zn_{0.7}Fe_2O_4$, *J. Appl. Phys.,* Vol 53, 1982, p 2722-2724
6. R. Mitra, R.K. Puri, and R.G. Mendiratta, Magnetic and Electrical Properties of Hot-Pressed Ni-Zn-Li Ferrites, *J. Mater. Sci.,* Vol 27, 1992, p 1275-1279
7. T. Nakamura and Y. Okano, Low Temperature Sintered Ni-Zn-Cu Ferrites, *L. Phys. IV France,* Vol 7, 1997, p C1-C91
8. R. Lebourgois, J. Ageron, H. Vincent, and J.-P. Ganne, "Low Losses Ni Zn Cu Ferrites," presented at Eighth International Conference on Ferrites (ICF8) September 18, The Japan Society of Powder and Powder Metallurgy (Kyoto and Tokyo, Japan), 2000
9. G.F. Dionne and R.G. West, Magnetic and Dielectric Properties of $Ni_{0.65}Zn_{0.35}Fe_{2-x}Mn_xO_4$, *J. Appl. Phys.,* Vol 61, 1987, p 3868-3870
10. S.A. Poltinnikov, Some Magnetic Properties of Nickel-Cadmium Ferrite, *Sov. Phys. Solid State,* Vol 8, 1966, p 1144-1149
11. S.A. Mazen, M.H. Abdallah, B.A. Sabrah, and H.A.M. Hashem, The Effect of Titanium on Some Physical Properties of $CuFe_2O_4$, *Phys. Status Solidi A,* Vol 134, 1992, p 263-271
12. F. Petil and M. Lenglet, Spectroscopic Evidence of the Mn^{3+}-Fe^{2+} Octahedral Pair in Lithium-Manganese Ferrites Near the Order-Disorder Transition, *Solid State Commun.,* Vol 86, 1993, p 67-71
13. R.D. Shannon and C.T. Prewitt, Revised Values of Effective Ionic Radii, *Acta Crystallogr.,* Vol B26, 1970, p 1046-1067
14. B.S. Boyanov, Synthesis and Neel Temperature Determination of Ferrites From the Mo-Zn-Fe_2O_3 Systems (M = Cu, Co and Ni), *J. Therm. Anal.,* Vol 41, 1994, p 1607
15. W.D. Kigery, H.K. Bowen, and D.R. Uhlmann, *Introduction of Ceramics,* John Wiley & Sons, 1975

16. N. Rezlescu, E. Rezlescu, C. Pasnicu, and M.L. Craus, Effect of the Rare-Earth Ions on Some Properties of a Nickel-Zinc Ferrite, *J. Phys.: Condens. Matter,* Vol 6, 1994, p 5707-5716
17. R.G. Kulkarini and V.U. Patial, Magnetic Ordering in Cu-Zn Ferrite, *J. Mater. Sci.,* Vol 17, 1982, p 843
18. S. Chikazumi and S. Charap, *Physics of Magnetism,* John Wiley & Sons, 1964, p 153
19. A.A. Sattar, A.H. Wafik, K.M. El-Shokrofy, and M.M. El-Tabey, Magnetic Properties of Cu-Zn Ferrites Doped With Rare Earth Oxides, *Phys. Status Solidi A,* Vol 171, 1999, p 563-569
20. G.C. Jain, B.K. Das, R.S. Khanduja, and S.C. Gupta, Effect of Intragranular Porosity of Initial Permeability and Coercive Force in a Manganese Zinc Ferrite, *J. Mater. Sci.,* Vol 11, 1976, p 1335-1338
21. S. Chikazumi and S. Charap, *Physics of Magnetism,* John Wiley & Sons, 1964, p 140
22. C.M. Srivastava, G. Srinivasan, and N.G. Nanadikar, Exchange Constants in Spinel Ferrites, *Phys. Rev. B: Condens. Mater,* Vol 19 (No. 1), 1979, p 499-508
23. J. Smit and P.J. Wijn, *Ferrites,* John Wiley and Sons, 1959, p 233